Modeling the effect of packing density on filtration performances in hollow fiber microfiltration module: A spatial study of cake growth

Jan Günther[a,b,*], Daniel Hobbs[b], Claire Albasi[a], Christine Lafforgue[b], Arnaud Cockx[b], Philippe Schmitz[b]

[a] *Laboratoire de Génie Chimique, UMR CNRS 5503, 5 rue Paulin Talabot, BP 1301, 31106 Toulouse Cedex 01, France*
[b] *Laboratoire d'ingénierie des Systèmes Biologiques et des Procédés, UMR INSA CNRS 5504, UMR INSA INRA 792, 135 avenue de Rangueil, 31077 Toulouse Cedex 04, France*

Keywords:
Hollow fiber
Cake
Packing density
Microfiltration
Backwash

A B S T R A C T

This study continues from a previous work on the impact of packing density on the fluid flow distribution in a hollow fiber module [1].

A numerical model was developed to simulate the growth of a particle cake along the surface of a hollow fiber membrane and the subsequent fluid flow during a microfiltration operation. The model accounts for the continuous change in porous domain (cake and porous wall) geometry and permeability as long as filtration occurs. The effect module packing density has upon cake growth is carefully analyzed both for inside/out (I/O) and outside/in (O/I) filtration modes. The results exhibit significant differences in the time variations of cake spatial distribution along the fiber as a function of packing density for both filtration modes. Then a confrontation between forward filtration and backward filtration velocities offers some conclusion on the effect of packing density on the backwash efficiency. This in turn underlines the importance of design parameters in the filtration performance of a hollow fiber module.

1. Introduction

Microfiltration membranes are used in a variety of particle separation processes, ranging from turbidity removal from waste water [2,3] to haze removal from wine, beer and fruit juice [4]. Hollow fiber modules have become ubiquitous not only due to their low manufacturing cost and simple handling but also for their high membrane area per unit volume of module, compared to other membrane configurations. Moreover, due to their low aspect-ratio hollow fiber membranes offer high mechanical strength and backwashing capability at low module energy costs, compared to alternatives such as plate-and-frame, spiral wound or tubular membranes.

However this module configuration has some disadvantages at high packing densities. Hollow fiber modules need empty spaces among fiber bundles and around each fiber, not only for the flow of the permeate, but also to facilitate the mass transfer between the fiber at the heart of the bundle to the periphery. For high packing densities, mass transfer and permeate flow could be limited.

Many authors have studied experimentally the influence of fiber bundle characteristics in microfiltration performance and particularly the impact of packing density on permeate flux [6–13]. Hollow fiber membrane modules can provide an extremely high filtration area mainly because of the high packing density of low-diameter hollow fibers. Wu and Chen [7] have studied the contribution from flow distribution on shell-side mass transfer performance in randomly packed hollow fiber modules. They observed that the mass transfer coefficients rapidly decreased with increasing packing density until the volume fraction reached 50%. It then increased with higher packing densities. The fiber packing density could change shell-side mass transfer coefficient as much as five fold in a hollow fiber module used for water degassing. Zheng et al. [9] have analyzed the effects of the fiber distribution or fiber random packing, on the mass transfer coefficient for a parallel flow module. They found a misdistribution of fluid flow in the shell side of the randomly packed hollow fiber module that became more apparent when the packing density was increased. Chang and Fane [6] experimentally studied the influence of fiber diameter on filtration and flux distribution in hollow fiber modules for cases with gas/liquid two phase flows. They also examined the influence of fiber arrangement; two kinds were studied with 4 and 8 fibers, and for two channel widths (24 and 8 mm). They showed that an increased fiber density decreased the rate of flux decline. They linked this phenomenon to a decrease in bubble size and a deteriorating inter-fiber hydrodynamic environment.

High packing densities can also promote fouling phenomenon due to the unfavourable hydrodynamic conditions within the fibers [8]. Flux decline is a ubiquitous feature of membrane separation

* Corresponding author at: Laboratoire d'ingénierie des Systèmes Biologiques et des Procédés, UMR INSA CNRS 5504, UMR INSA INRA 792, 135 avenue de Rangueil, 31077 Toulouse Cedex 04, 5 France.
E-mail address: jan.gunther@insa-toulouse.fr (J. Günther).

processes due to an accumulation of retained material in the form of a cake or a precipitate at the membrane surface or from adsorption within the membrane pores that increases the membrane filtration resistance. In dead-end microfiltration systems, the flux decline depends on various features of the feed stream that influence the filtration resistance of the retained cake [14,15]. For hollow fiber membrane systems, the flux decline mechanisms are even more complex. Several causes can be described and pressure drop gradients are considered first.

For a vertically mounted hollow fiber membrane module operating in outside/in filtration mode, when pressure is applied to the external side of the fiber (to obtain permeate flow through the porous membrane) some of the internal pressure drop will occur along the membrane while permeate flows in the fiber lumen. The local transmembrane pressure, which is obtained from the difference between outside and inside pressure, is higher at the exit and lower at the entrance of flow. The local flux at the permeate exit is therefore higher resulting in more rapid membrane fouling in this area [6]. These flux gradients depend upon fiber design characteristics such as fiber length, fiber diameter and membrane permeability [8].

In literature, different two dimensional numerical models have been described to simulate the flow in a membrane or thin channels with permeable walls [8,16–20]. Some authors have based their models on a module design in which the position of the feed inlet creates a radial pressure drop, i.e., inflow is via a tube situated at the centre of the bundle [21,22], or at the inlet of the outer surface of the bundle. These models however, generally underestimate the pressure drop due to packing density.

The computational fluid dynamics based model developed in our previous work [1], has explored the impact of geometrical parameters of hollow fibers on the filtration performances of ultrapure water of the module. An axisymmetric 2D model operating in dead-end filtration mode has underlined the major effects of packing density on the pressure profile and spatial distribution of permeate velocity along the fiber length. In this study, a numerical model was developed to simulate the growth of a particle cake along the surface of a hollow fiber membrane and the subsequent fluid flow during a microfiltration operation of particles in the context of a microorganism separation. The model accounts for the continuous change in permeability and the geometry of the fluid and porous domains during filtration. Numerical simulations were performed to study the particular case of a hollow fiber module that is usually used in a particular experimental device [27]. The hollow fiber module is used inside a membrane bioreactor that was previously designed to study microbial interactions [5]. In this device, a physical separation of the different microbial species in two tanks is obtained thanks to the hollow fiber module. Thus, the growth of each microbial species is easily analyzed as pure cultures. However, in order to ensure environmental conditions similar to ones obtained if all the microorganisms were in a same reactor, filtration stage should not be restrictive for biological kinetics and all soluble compounds taking part in microbial activity must cross the membrane.

For this device, in the same way as other fiber bundles in many different applications, studies have shown the significant effect of hydrodynamics on filtration performances and on the growth of a fouling cake. Consequently, in order to get the best separation performances the module design should be optimized taking into account the links between its geometry, hydrodynamics and fouling.

Firstly we present the geometrical domain and the associated set of governing equations for fluid. Secondly we carefully detail the model developed to account for cake formation in the case of spherical monodispersed particles (modeling yeast cells). Then the simulation results are presented and discussed in terms of time variations and spatial distribution of particle cake along the fiber both for inside/out (I/O) and outside/in (O/I) filtration mode. Finally some recommendations are given to improve not only the filtration stage but also the backwash stage.

Table 1
Summary of parameters values used for numerical model.

r_i	$125e^{-6}$ m
r_e	$210e^{-6}$ m
L	0.125 m
e_m	85 μm
K_m	$1.7e^{-16}$ m^2
d_p	$5e^{-6}$ m
D/Φ	$25e^{-6}$ m/$0.850e^{-6}$ m/$0.6100e^{-6}$ m/0.4
$P_L - P_0$	±0.8 bar

2. Methods

2.1. Flow model

A model based on the finite element method was developed in a previous paper [1] to simulate numerically the flow in a dead-end hollow fiber module. For the sake of clarity we briefly recall the geometrical domain, the governing equations and the associated boundary conditions of the aforementioned model.

Assuming a regular arrangement and a homogeneous working of the fibers in the module, the geometrical domain is simplified as a unit element of the module, i.e., a single hollow fiber of length L. An annular region of fluid surrounding the fiber is considered in order to account for the packing density of the module according to the classical Happel's free surface model [24]. The final domain is therefore axisymmetric and consists of two cylindrical fluid regions (i and o) separated by a porous region (p) as depicted in Fig. 1.

The inner and outer radii of the hollow fiber are r_i and r_e, respectively and the thickness of the fluid envelope surrounding the fiber is D. The ratio "fluid volume to solid volume" in the single cell model is taken equal to the ratio "fluid volume to solid volume" in the entire module, when considering all the fiber. The characteristics parameters of the fiber modules and the operating conditions (fiber size, pressure value) studied in the paper are reported in Table 1. These values are based on the experimental conditions used in previous experimental studies [1,23].

We consider a stationary, laminar and incompressible flow of a Newtonian fluid in the inner (k = i) and outer fluid channels (k = o). The Navier Stokes equations govern the mass and momentum balances:

$$\nabla . u^k = 0 \tag{1}$$

where ρ is the fluid density, μ is the fluid dynamic viscosity, P is the pressure, and u is the velocity vector. The flow in the porous domain p is ruled by the Darcy Brinkman equation as follows:

$$\rho . \frac{\partial u^k}{\partial t} + \rho(u^k . \nabla u^k) = -\nabla p^k + \mu \nabla^2 u^k \tag{2}$$

where ρ is the fluid density, μ is the fluid dynamic viscosity, p is the pressure, and $\boldsymbol{u}$ is the velocity vector. The flow in the porous domain p is ruled by the Darcy Brinkman equation as follows:

$$\frac{\rho}{\varepsilon} . \frac{\partial u^p}{\partial t} + \mu_{eff} \nabla^2 u^p - \nabla p^p - \frac{\mu}{K_t} u^p = 0 \tag{3}$$

where μ_{eff} is the effective dynamic viscosity, commonly considered as μ/ε, ε representing the porosity and K_t is the intrinsic permeability of the porous domain. It is noted that the Darcy model is perfectly adequate to model fluid flow in porous media however, the Darcy Brinkman model is preferred when coupling fluid and porous flow problems, in particular in the transition region where the continuity can thus be preserved for $\boldsymbol{u}$ and its derivatives.

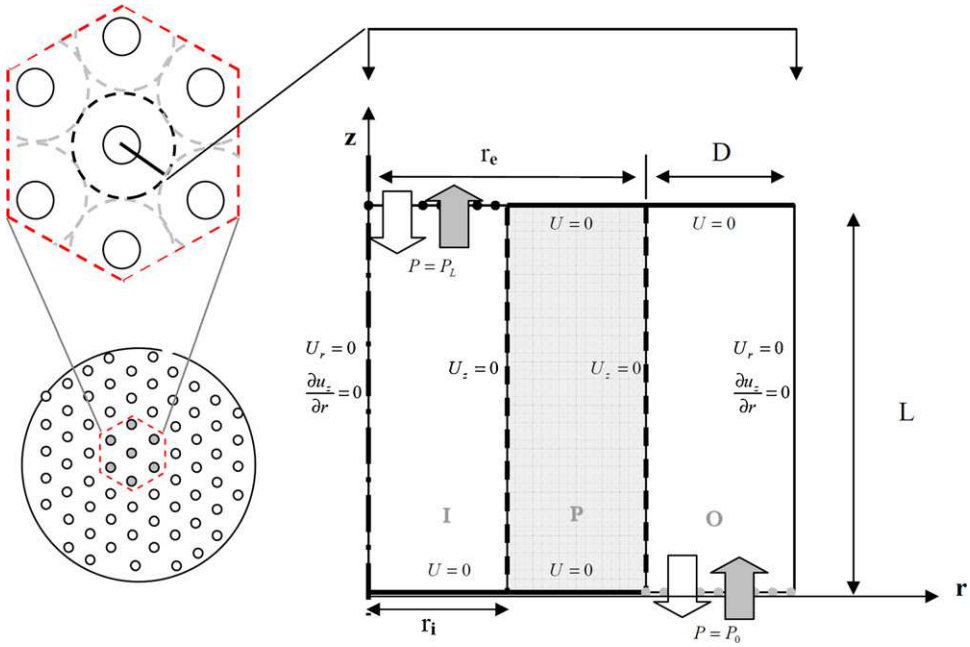

Fig. 1. Geometrical simplification of the hollow fiber bundle and scheme of the model with I: internal channel, M: membrane, E: external channel, R_{ext}: outer radius, D: distance between two fibers, L: length of the fiber.

The associated boundary conditions were chosen to represent a real application, i.e., constant working pressure, where the overall pressure difference between inlet and outlet is specified. Constant pressure values are therefore considered at the inner fluid region inlet and the outer fluid region outlet. The free surface condition, proposed by Happel [24], is assumed at the external boundary of the outer fluid region. It is also assumed that there is a no slip velocity at the fluid/porous interface [25]. Finally the whole boundary conditions with respect to r and z axis, summarized in Fig. 1, can be written as:

Inner fluid region:

$$p^{\mathrm{i}}(0 \le r \le r_{\mathrm{i}}, z = L) = P_L \tag{4a}$$

$$u_z^{\mathrm{i}}(0 \le r \le r_{\mathrm{i}}, z = 0) = 0 \tag{4b}$$

$$u_r^{\mathrm{i}}(0 \le r \le r_{\mathrm{i}}, z = 0) = 0 \tag{4c}$$

$$\frac{\partial u_z^{\mathrm{i}}}{\partial r}(r = 0, 0 \le z \le L) = 0 \tag{4d}$$

$$u_r^{\mathrm{i}}(r = 0, 0 \le z \le L) = 0 \tag{4e}$$

Outer fluid region:

$$p^{\mathrm{o}}(r_{\mathrm{e}} \le r \le r_{\mathrm{e}} + D, z = 0) = P_0 \tag{5a}$$

$$u_z^{\mathrm{o}}(r_{\mathrm{e}} \le r \le r_{\mathrm{e}} + D, z = L) = 0 \tag{5b}$$

$$u_r^{\mathrm{o}}(r_{\mathrm{e}} \le r \le r_{\mathrm{e}} + D, z = L) = 0 \tag{5c}$$

$$\frac{\partial u_z^{\mathrm{o}}}{\partial r}(r = r_{\mathrm{e}} + D, 0 \le z \le L) = 0 \tag{5d}$$

$$u_r^{\mathrm{o}}(r = r_{\mathrm{e}} + D, 0 \le z \le L) = 0 \tag{5e}$$

Porous region:

$$u_z^{\mathrm{p}}(r_{\mathrm{i}} \le r \le r_{\mathrm{e}}, z = L) = 0 \tag{6a}$$

$$u_r^{\mathrm{p}}(r_{\mathrm{i}} \le r \le r_{\mathrm{e}}, z = L) = 0 \tag{6b}$$

$$u_z^{\mathrm{p}}(r_{\mathrm{i}} \le r \le r_{\mathrm{e}}, z = 0) = 0 \tag{6c}$$

$$u_r^{\mathrm{p}}(r_{\mathrm{i}} \le r \le r_{\mathrm{e}}, z = 0) = 0 \tag{6d}$$

Porous/fluid interface:

$$u_r^{\mathrm{p}}(r = r_{\mathrm{e}}, 0 \le z \le L) = u_r^{\mathrm{o}}(r = r_{\mathrm{e}}, 0 \le z \le L) \tag{7a}$$

$$p^{\mathrm{p}}(r = r_{\mathrm{e}}, 0 \le z \le L) = p^{\mathrm{o}}(r = r_{\mathrm{e}}, 0 \le z \le L) \tag{7b}$$

$$u_z^{\mathrm{p}}(r = r_{\mathrm{e}}, 0 \le z \le L) = u_z^{\mathrm{o}}(r = r_{\mathrm{e}}, 0 \le z \le L) = 0 \tag{7c}$$

$$u_r^{\mathrm{p}}(r = r_{\mathrm{i}}, 0 \le z \le L) = u_r^{\mathrm{i}}(r = r_{\mathrm{i}}, 0 \le z \le L) \tag{7d}$$

$$p^{\mathrm{p}}(r = r_{\mathrm{i}}, 0 \le z \le L) = p^{\mathrm{i}}(r = r_{\mathrm{i}}, 0 \le z \le L) \tag{7e}$$

$$u_z^{\mathrm{p}}(r = r_{\mathrm{i}}, 0 \le z \le L) = u_z^{\mathrm{i}}(r = r_{\mathrm{i}}, 0 \le z \le L) = 0 \tag{7f}$$

where the superscripts i, o, and p are used for inner fluid, outer fluid and porous regions, respectively, and the subscripts z and r indicate the axial and radial velocity components, respectively.

It can be noticed that $P_L - P_0$ is positive or negative in inside/out filtration mode (IO) or outside/in filtration mode (OI), respectively.

2.2. Fouling model

The development of the fouling model begins by considering the fouling of a plain filter medium – the membrane – in a cake filtration operation. It is commonly assumed that the total resistance of the fouled membrane R_t is the sum of two resistances given by:

$$R_t = R_{\mathrm{m}} + R_{\mathrm{f}} \tag{8}$$

where R_{m} is the intrinsic resistance of clean membrane and R_{f} is the fouling layer resistance.

Firstly it is assumed that: (i) there is separation of the scales, i.e., the particle size is much larger than the pore size and secondly; (ii) the fluid flow is uniform at the membrane surface. These assumptions can fail in some complex cases [26,27] where the total resistance is actually an order of magnitude higher than that obtained by Eq. (8) at the beginning of filtration. The fouling resistance is null for a clean membrane but will increase as filtration occurs. R_{f} can be considered as the sum of the external and internal fouling resistances. The external fouling resistance is due to a cake layer formed by the accumulation of particles at the membrane surface. The internal fouling resistance is due to pore blocking and pore constriction. For simplicity, due to the differences in pore and

particle size, it is assumed that the internal resistance is negligible in the present study. Thus fouling is only considered as the consequence of the accumulation of large particles – micro-organisms in the considered application – at the surface of the membrane. Moreover, particles are supposed to be monodispersed and spherical. This can be a reasonable approximation for some microorganisms such as *Saccharomyces cerevisiae*. It is true that it is a drastic simplification for many other cases but we can thus make use of the Carman Kozeny model to evaluate cake resistance and thus focus our analysis on modeling the filtration at the fiber scale. However, this part of the modeling would certainly deserve to be significantly improved and it would be easy to incorporate any improvement in the modeling at the plane filter medium scale in our approach. The hydraulic resistance of a cake layer made of monodispersed spherical particles is given by the Carman Kozeny model [28]:

$$R_c = \frac{150 e_c (1-\varepsilon_c)^2}{d_p^2 \varepsilon_c^3} \tag{9}$$

where d_p is the particle diameter and e_c and ε_c are the thickness and the porosity of the cake layer, respectively. Therefore the total resistance of the fouled membrane becomes:

$$R_t = R_m + R_c \tag{10}$$

The thickness of the cake layer e_c can be calculated from the mass of particles deposited per unit area as:

$$e_c = \frac{m_p}{\rho_p (1-\varepsilon_c)} \tag{11}$$

where ρ_p is the density of particles and is considered similar to that of the fluid. Hence in this approach, the cake is characterised by one single parameter: its porosity ε_c. Furthermore it is assumed that the cake is not compressible and its porosity is constant and uniform.

The next step consists of combining the fouling model for the plain filter medium with the flow model described in Section 2.1 to model the filtration at the fiber scale.

During the filtration process, particles are transported by the fluid towards the membrane. Particle motion depends on several mechanisms such as convection, Brownian diffusion, gravity and inertia [29]. Gravity effect can be neglected as particles are non-buoyant [34]. The relative magnitude of Brownian diffusion and inertia compared to convection can be estimated using the two following dimensionless numbers: Peclet, P_e and Stokes, S_t numbers expressed as:

$$P_e = \frac{6\pi\mu U_f d_p^2}{kT} \tag{12}$$

$$S_t = \frac{\rho_p U_f d_p^2}{18\mu l} \tag{13}$$

where u_f is the characteristic filtration velocity, k the Boltzmann constant, T is the temperature and l is a characteristic length scale of the fluid domain (r_i for I/O and D for O/I filtration modes, respectively). Using the typical data for the considered application gives $P_e > 10^3$ and $S_t < 10^{-5}$ and indicates that both Brownian diffusion and inertia have a negligible effect on the particles motion. Therefore, on the basis of the above estimates, it is assumed that particles follow the streamlines until they make contact with the membrane or the cake. Moreover, the molecular interaction forces allow particles to adhere as soon as they make contact. The particle deposition rate is then simply proportional to the local filtration velocity. As a result of the particle capture, a filtration cake eventually forms at the membrane surface. This induces a modification of the free fluid domain since the channel aperture decreases as the cake grows. This in turn results in the evolution of the free fluid flow within the entrance channel (inner fiber in I/O or outer fiber in O/I filtration modes, respectively) due to the modification of both the free fluid domain geometry and filtration velocity distribution along the membrane. These effects are accounted for in the model under the assumption of a quasi-steady evolution of the entrance channel flow. This assumption is supported by the fact that the travel time of a particle in the entrance channel is much smaller than the time needed for observing a significant change in the filtration cake local thickness.

2.3. Numerical method

The set of equations (1)–(7) is solved using the commercially available finite element code COMSOL multiphysics™. To compute the evolution of filter medium properties as far as filtration occurs, inner fiber radius (I/O filtration modes) or outer fiber radius (O/I filtration modes) is no longer uniform and constant but becomes time dependant and varies all along the z axis.

The method used to account for particle deposition and cake layer in the simulations is identical for I/O and O/I filtration modes. So let us consider for instance the I/O filtration mode. As discussed in Section 2.2, the particle deposition rate can be assumed to be proportional to the local filtration velocity. Thus the time variation of mass of particles deposited per unit area at time t at the position z along the membrane is equal to the convective flux of mass of particles. This can be expressed as:

$$\frac{dm_p}{dt}(z,t) = C_p u_r^i(r = r_i, z, t) \tag{14}$$

where C_p is the particle concentration in the fluid (kg/m^3).

Cake growth, resulting from the mass of particles deposited, is modeled using a mesh deformation method, named A.L.E (Arbitrary Lagrangian and Eulerian method). This method aims to increase the porous domain constituted by the porous wall (membrane) and the cake layer and to decrease the inner fluid domain with respect to cake layer thickness without any remeshing [30]. The permeability and the thickness of the new porous domain are no longer uniform and constant and vary with respect to Eqs. (9)–(11) as follows:

$$\frac{e_t(z)}{K_t(z)} = R_c(z) + R_m \tag{15a}$$

$$e_t(z) = e_c(z) + e_m \tag{15b}$$

where K_t is the permeability of the porous domain (instead of K_m) and e_t is the thickness of the porous domain (instead of e_m).

From a technical point of view, the velocity component of the fluid–cake interface in the r-axis direction, u_r^c has to be considered. It is simply derived from Eq. (11):

$$u_r^c(z) = -\frac{dm_p/dt}{\rho_p.(1-\varepsilon_c)} \tag{16}$$

Then using Eq. (14), we obtain:

$$u_r^c(z) = -\frac{C_p}{\rho_p.(1-\varepsilon_c)} u_r^i(r = r_i, z) \tag{17}$$

It can be noticed that the negative sign indicates that the fluid–cake interface moves towards the centreline of the fiber (I/O filtration mode). In O/I filtration mode, the method is the same and u_r^c is be written as:

$$u_r^c(z) = \frac{C_p}{\rho_p.(1-\varepsilon_c)} u_r^o(r = r_e, z) \tag{18}$$

The A.L.E. model is solved at each time step to calculate the new mesh, using u_r^c as the boundary condition at the interface of the fluid/porous domain meshes (inner fiber side for I/O and outer fiber side for O/I, respectively). It means that the displacement velocity of the mesh is prescribed at the fluid/porous domain interface

in the direction of cake growth. In addition, a free mesh displacement in the radial direction is required at $z=0$ and $z=L$ in the fluid domain in which the cake develop. Finally a condition of no mesh displacement is imposed at the other boundaries.

Numerical computations are finally performed according to the following steps:

- At $t=0$: $K_t(z)=K_m$ and $e_t(z)=e_m$. Fluid flow is computed in both fluid and porous domains.
- At $t=\Delta t$: $m_p(z)$ and $e_c(z)$ are calculated from $u_r^i(r=r_i,z)$. Then $K_t(z)$, $e_t(z)$, $u_r^c(z)$ are also calculated.
- The mesh and then the size of the fluid domain (inner fiber for I/O and outer fiber for O/I, respectively) and of the porous domain are changed using A.L.E. model and fluid flow is computed in the new domains.
- and so on.

The time dependant solver is used with a direct linear system solver (PARDISO) and the time step is free taken by the solver but controlled by a relative tolerance of 1% for an accurate transient simulation. In our case, this time step ensures an increase of the cake thickness always lower than one monolayer of particle (about 5 μm).

To sum up, the assumptions that were done in this study are listed below:

- Shear-induced cake removal as observed in cross-flow or submerged filtration model was not included. Moreover, back-transport phenomena based on diffusion were neglected. According to these assumptions, the particles follow stream lines until approaching the membrane or the cake surface, where they form a deposit. For this typical device, the filtration could be assimilated as dead end filtration. The shear induced cake removal was neglected because the fluid flow velocity in the z direction remained small compared to the fluid flow in r direction.
- The particles were envisioned as non-buoyant, monodisperse spheres, which formed cakes of homogeneous porosity. Phenomena such as pore blocking or cake compressibility were not taken into account. The spherical particles (7 μm diameter) are more than 10 times the size of the pore (0.1 μm), so pore blocking was not taken in account.
- The void fraction of a hollow-fiber bundle was represented as an outer fluid region with a thickness was corresponding to the packing density. This fluid region was assumed to be of annular shape, thus neglecting fiber–fiber contacts as observed for an irregular fiber arrangement. In our previous study we have shown good agreement between this 1D model and experimental data which validate this last assumption.

2.4. Calculation mesh

Typically, a mesh with 100 cells along the fiber, 20 cells across the inner channel, and 10 cells across the porous medium were used. For the external annular channel, 5 cells, 10 cells and 20 cells were used for diameters of $D=25$ μm, $D=50$ μm and $D=100$ μm, respectively. Moreover, a non uniform mesh distribution was used for internal and external channel, with the cell density being higher at the membrane interface. Special care was taken to avoid excessively high cell stretch rates. In all the three cases, we checked that the filtration velocity profile along the fiber and flow rate of the external channel were independent of the mesh used. Using a mesh five times smaller, the difference was below 0.2% and 0.04%, respectively for the filtration velocity and for the flow rate values. From these results, we choose a grid containing:

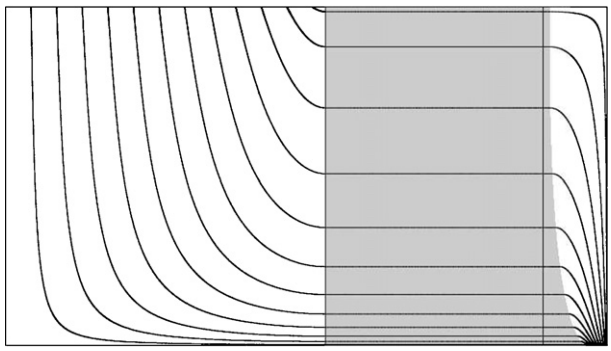

Fig. 2. Numerical simulations performed using flow model and fouling model in outside/in filtration mode.

- 3250 elements for $D=25$ μm ($\Phi=0.8$),
- 3450 elements for $D=50$ μm ($\Phi=0.6$) and
- 4950 elements for $D=100$ μm ($\Phi=0.4$).

3. Results

Numerical simulations performed using the flow (Section 2.1) and fouling (Section 2.2) models are illustrated in Fig. 2, where a typical outside/in filtration is presented. After a certain filtration time, a non-uniform cake developed on the outer fiber surface. The membrane and cake create a non-uniform porous region (in light grey in Fig. 2) that separates the inner and outer fluid regions. The streamlines (straight lines) show the fluid flow from the entrance (bottom of the outer fluid region, i.e., the outer fiber) to the exit (top of the inner fluid region, i.e., the inner fiber) of the system. In this particular case, the computational results indicate that filtration preferentially takes place close to the entrance since streamlines are more tightly packed at the bottom than at the top of the porous region.

As already mentioned, all the numerical simulations were performed for a constant and uniform cake porosity $\varepsilon_c=0.45$. The results are presented and discussed in terms of filtration velocity v_f (m/s) and cake thickness e_c (m) along the fiber length. The filtration velocity is defined as the radial velocity at the inner fluid/porous interface for I/O filtration ($u_f(z)=u_r^p(r_i,z)=u_r^i(r_i,z)$) and at the outer porous/fluid interface for O/I filtration ($u_f(z)=u_r^p(r_e,z)=u_r^o(r_e,z)$. In the associated figures, the bottom of the fiber corresponds to the $z=0$ position and the top is the $z=L$ position. For I/O the suspension entrance is at the top of the fiber while for O/I the flow circulates from the bottom to the top of the fiber.

3.1. Inside/out filtration mode

Longitudinal profiles of filtration velocity: (i) with pure water and (ii) with a particle suspension are shown in Fig. 3. For pure water filtration, previous work [1] has shown that space restriction in the annulus due to an increase in packing density, leads to a higher pressure at the top of the external channel than at the bottom. This phenomenon generates a high local transmembrane pressure gradient along the fiber that governs the flux value (Fig. 3a). Thus, filtration takes place preferentially in the region where the local transmembrane pressure is higher. The filtration flow velocity is 70% higher at the bottom of the fiber than at the top with a high packing density ($\Phi=0.8$). Conversely, filtration preferentially takes place at the top of the fiber with a low packing density ($\Phi=0.4$) leading to a filtration flow velocity 25% higher.

When an actual filtration takes place (where the fluid contains particles), the cake formation modifies the longitudinal profile of the filtration flow velocity. The plots in Fig. 3b–d illustrate the

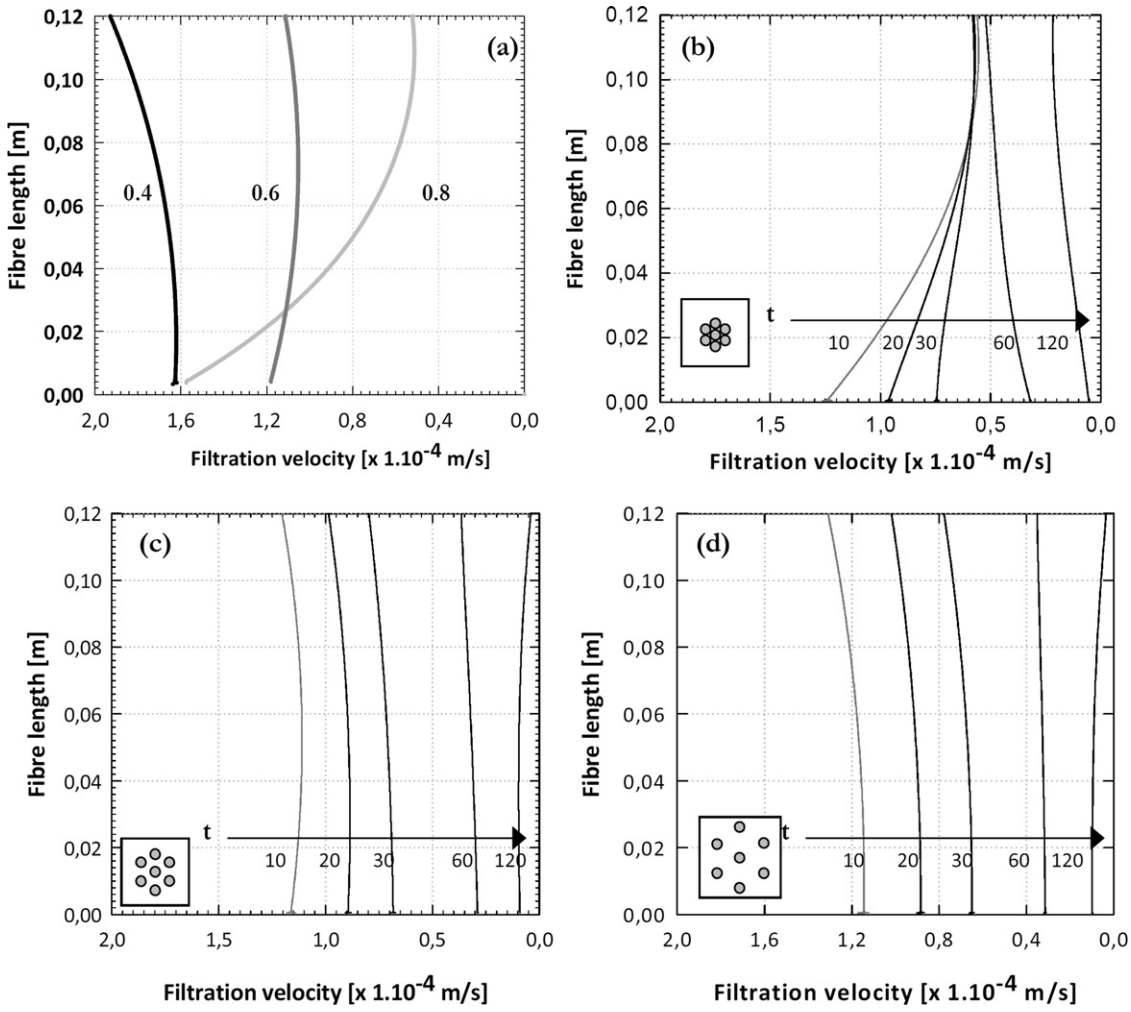

Fig. 3. Axial flux profiles for IO filtration mode without particles (a), and for fouling of the fiber for three packing densities with time: (b) $\Phi = 0.8$, (c) $\Phi = 0.6$, (d) $\Phi = 0.4$.

decline in filtration velocity from when $t = 10$ s to $t = 120$ s for the three packing densities.

For the highest packing density ($\Phi = 0.8$) (Fig. 3b), the filtration velocity is lower towards the entrance of the fiber flow than at the bottom due to a lower local transmembrane pressure. The time variations of the longitudinal profile show a homogenization of the filtration velocity along the fiber in the first minute and then a slight change in the flow profile probably due to the cake characteristics (thickness). Fig. 4a shows that the cake deposit is thicker at the bottom of the fiber by 50% after 10 s and 10% after 120 s. Considering a medium packing density of $\Phi = 0.6$ (Fig. 3c), the variation in the filtration flow velocity along the fiber remains low. However, at the beginning of the filtration, the filtration flow velocity is slightly higher near the entrance and at the bottom of the fiber during the first 10 s. The profile becomes more homogeneous after 30 and 120 s. This tendency is confirmed in Fig. 4b which reveals a higher cake thickness at both extremities of the fiber at the initial stage of filtration and a homogeneous cake thickness at the final stage. When considering the lowest packing density ($\Phi = 0.4$), the situation is opposite to that obtained for the highest packing density. The filtration velocity is higher at the top of the fiber leading to a thicker cake near the entrance. The results for this latter case are close to those for filtration models described in literature [31,32].

3.2. Outside/in filtration mode

The filtration flow velocity profile along the fiber with pure water (i) and a particle suspension (ii) are shown in Fig. 5. Fig. 5a summarizes the flow velocity obtained without particles, i.e., at the beginning of the filtration step and illustrates how packing density affects filtration flow velocity profile along the fiber length. Due to pressure variations along the fiber, the greatest variation in the flow velocity profile along the fiber is experienced with the highest packing density where as it is more homogeneous with a medium fiber packing density.

When filtering a particle suspension, the longitudinal filtration flow velocity profile drastically changes with time as the cake grows. With the highest packing density, the flux reduction along the fiber length appears to be more important than for I/O filtration due to the local pressure conditions. Considering high (Fig. 5b) and medium (Fig. 5c) packing densities, at the beginning of filtration, the highest flow velocity values are first obtained in the inlet half of the hollow fiber. For fiber densities of $\Phi = 0.8$ and $\Phi = 0.6$, the filtration velocity is 80% and 10% higher near the entrance (at the bottom of the fiber), respectively. For a packing density of $\Phi = 0.4$, the filtration flow velocity profile is more homogeneous; filtration takes place all along the fiber rather than at the ends of the fiber, at both the beginning and end of the filtration simulation. These results show that a decreasing packing density leads to a

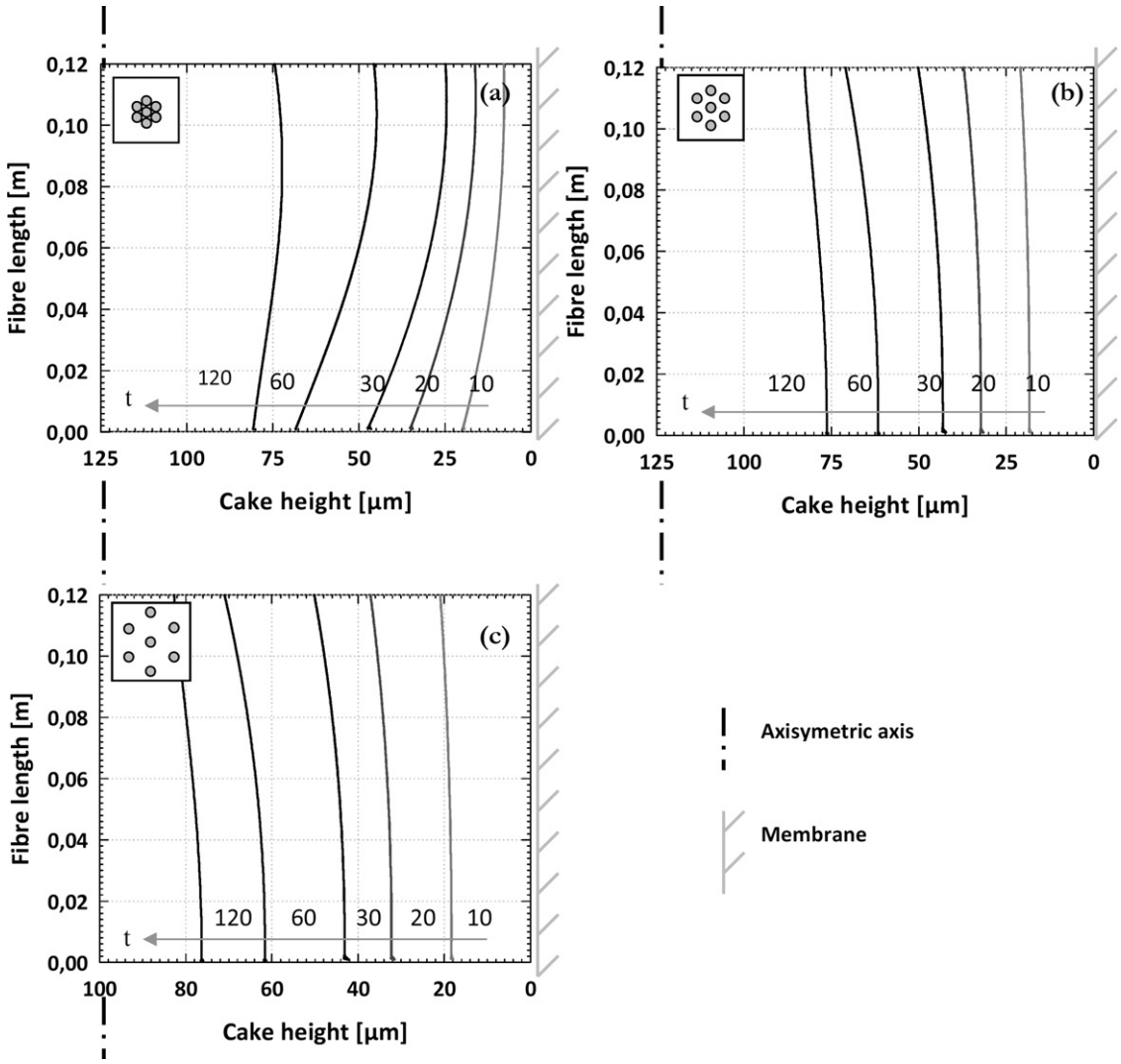

Fig. 4. Cake height profile for IO filtration mode. (a) $\Phi = 0.8$, (b) $\Phi = 0.6$, (c) $\Phi = 0.4$.

higher filtration flux and a more homogeneous flux profile along the fiber.

The spatial deposition of particles and the resulting cake growth along the fiber length is a direct consequence of the preferential flow profile described above. At the end of the filtration simulation, the cake becomes thicker when moving towards the bottom of the fiber and is more significantly so between the middle and the bottom of the fiber for the high and the medium packing densities to preserve its initial spatial distribution. Considering the lowest packing density, the cake growth is more or less uniform along the fiber with time due to the stability of the flux profile. The overall cake deposition along the fiber is more important but more homogeneous than the one obtained at higher packing densities.

The overall performance of the two filtration modes can be expressed by the net flow rate of one fiber Q (µl/s). This is derived from a simple integration of the filtration velocity over the membrane area as follows:

$$Q = 2\pi r_i \int_0^L u_r^i \, dz \tag{19}$$

The time variations of the flow rate values illustrate the strong influence of the filtration mode on filtration performance (Figs. 7 and 8) since for the I/O filtration mode the flux tends to level off while in the O/I filtration mode a continuous decrease is still present after 120 s.

For packing densities of 0.8 (Fig. 6a) and 0.6 (Fig. 6b), it is noted that the filtration stops at 20 s and 60 s, respectively. After these times, the cake is so thick at the entrance (the bottom) that it prevents the fluid from entering the outer region and therefore filtration stops. This phenomenon is illustrated in Fig. 8 the evolution of the filtration flow rate with time for the O/I filtration mode is presented. For packing densities of 0.8 and 0.6 the filtration stops as previously described at 20 and 60 s (arrow) with a flow rate equal to zero. For a packing density of 0.4, the filtration simulation reaches the designated filtration time of 120 s where the cake grows to a thickness of 75 µm along the whole fiber (Fig. 6c). This value is of the same order of magnitude obtained for the cake thickness for an I/O filtration of the same time. This suggests that for a packing density of 0.4, the pressure gradient is not large enough to overcome the combined resistances of the membrane and the cake at any point along the fiber and thus results in a very low filtration flux (<5 µl/s at 120 s) as shown in Figs. 7 and 8.

4. Discussion

The observed distinct patterns of cake deposition onto the membrane surface can be assumed to be a consequence of the

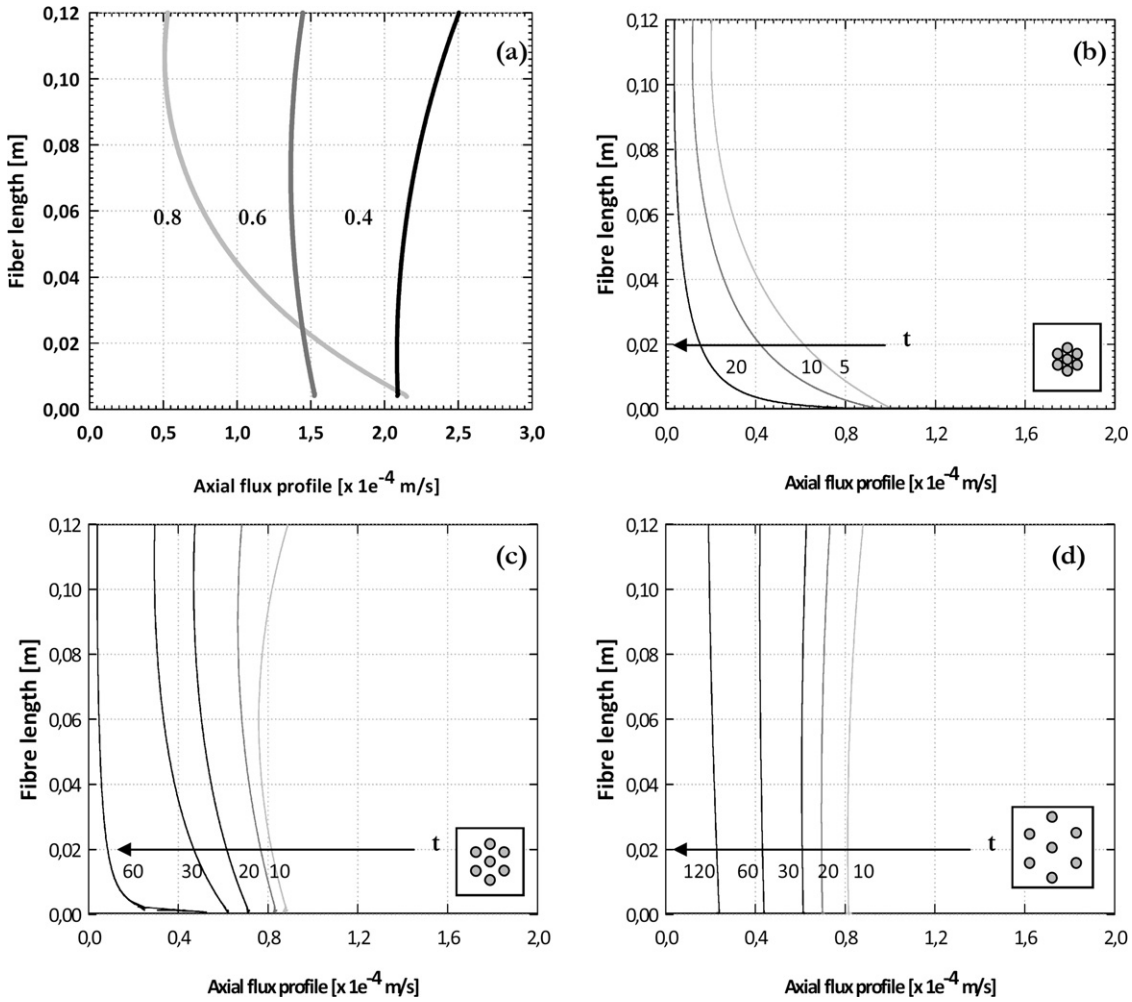

Fig. 5. Axial flux profiles for OI filtration mode without particles (a), and for fouling of the fiber for three packing densities with time: (b) $\Phi = 0.8$, (c) $\Phi = 0.6$, (d) $\Phi = 0.4$.

non-uniform filtration velocity profile which, appears to depend on the membrane permeability and fiber packing density as demonstrated previously [1]. The impact of the packing density on the fouling of the hollow fiber membranes could be described in three distinct mechanisms, characterised by preferential areas of particle deposition and cake growth along the fiber length.

(i) The first mechanism is related to the simple problem of filtration in a single porous tube with suction. With an I/O filtration mode and very low packing density, the fiber behaves as if it was a single fiber without neighbours, the filtration velocity along the fiber should then be independent of the packing density and the outer pressure is uniform. This mechanism is deduced from Fig. 3a (I/O filtration without particles) which, gives the longitudinal profile of filtration velocity at the beginning of the filtration and Fig. 4c which shows the time variations of the aforementioned profile during filtration. The highest flux is first obtained near the entrance of the fiber where the pressure difference is higher. This increases the particle deposition on membrane surface near the entrance. The flux profile and the subsequent cake growth then progressively become more uniform. It can be deduced from Fig. 4c that the difference between the maximum and minimum cake heights relative to the mean cake height, $|e_{c\ \max} - e_{\min}| / \langle e_c \rangle$, decreases with time.

(ii) The second mechanism is due to space restrictions in the external annulus, corresponding to the high packing density. The resulting filtration pattern is characterised in Figs. 4a and 6a, by preferential deposition of the particles between the middle and the bottom of the fiber. Consequently, the most productive region of the membrane, in terms of flux, is fouled first and the filtration velocity decreases more rapidly than for the rest of the fiber as shown in Figs. 3b and 5b. Nevertheless, the distribution of cake growth is different for the outside/in and in/outside filtration modes. This could be explained by a higher effect of external region restriction due to the existence of the deposit on the outer pressure.

(iii) The third mechanism describes how a more homogeneous filtration takes place along the fiber as the packing density decreases and the pressure distribution along the fiber in the external channel is more uniform. It can be assumed that part of the fiber membrane surface area that was not readily accessible at high packing density becomes accessible and active when the density decreases. As a result, the rate of cake growth is higher as shown in Fig. 4b and 6b however, this can have a negative effect on the filtration as the channel diameter will decrease quicker due to the increased cake deposition. This phenomenon is more pronounced with an outside/in filtration mode and is clearly illustrated by Fig. 6a and b. As the cake grows in the channel, the fluid flow cross section becomes smaller. At a critical moment occurs at 60 s, where the pressure distribution becomes similar to that obtained for a high packing density and then, the filtration mainly takes place near the entrance of the fiber (Fig. 5c, $t = 60$ s).

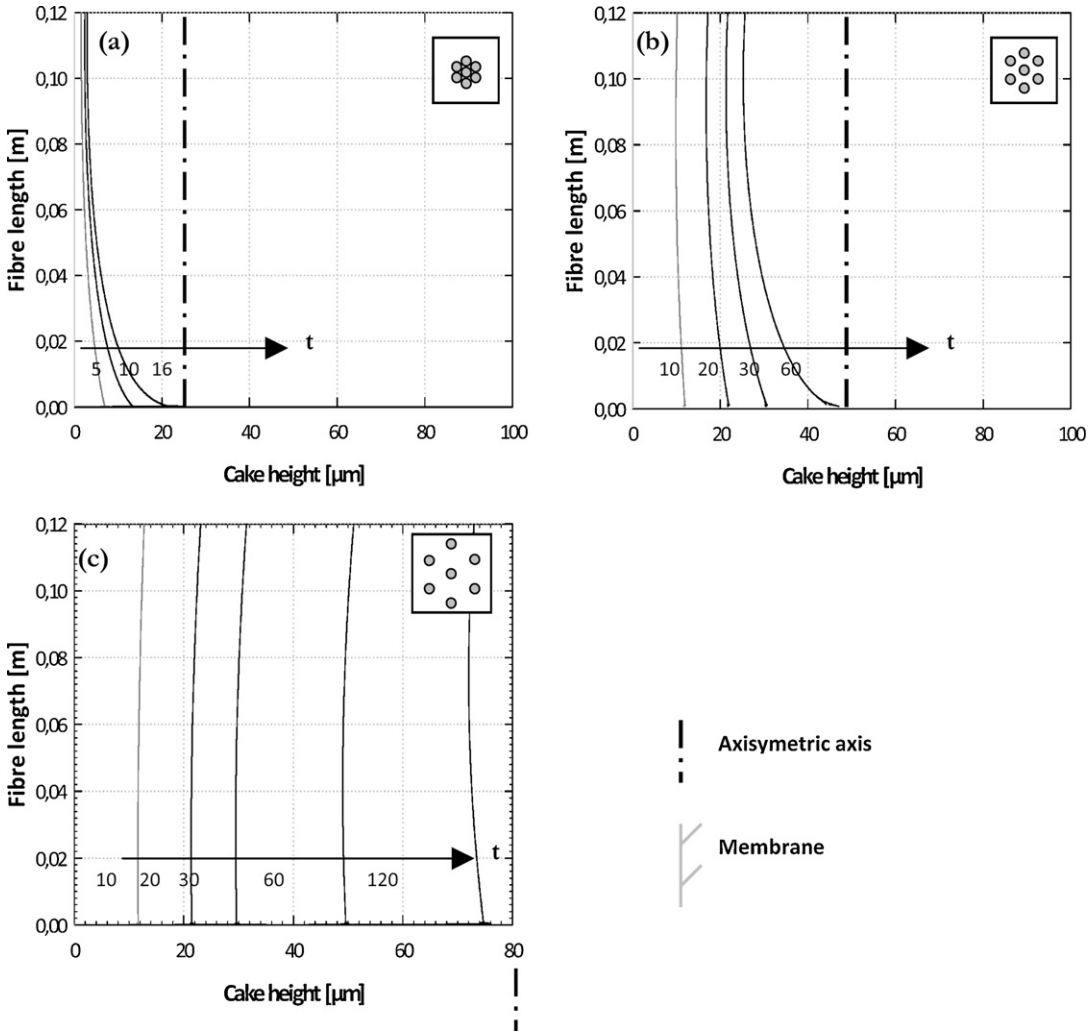

Fig. 6. Cake height profile for OI filtration mode. (a): $\Phi = 0.8$, (b) $\Phi = 0.6$, (c) $\Phi = 0.4$.

As described in the previous sections, Figs. 3a and 5a represent the longitudinal variations of the filtration velocity along the fiber without particles for the inside/out and outside/in filtration modes, respectively. Fig. 4 and 6 represent the cake thickness profiles for the inside/out and outside/in filtration modes, respectively. It can be noticed that in the context of the application of interest which is an immersed membrane bioreactor [5], the resistance of the cake was less than the resistance of the membrane.

Indeed, for this fluid, the cake and membrane resistance were measured experimentally and it was shown that the cake resistance

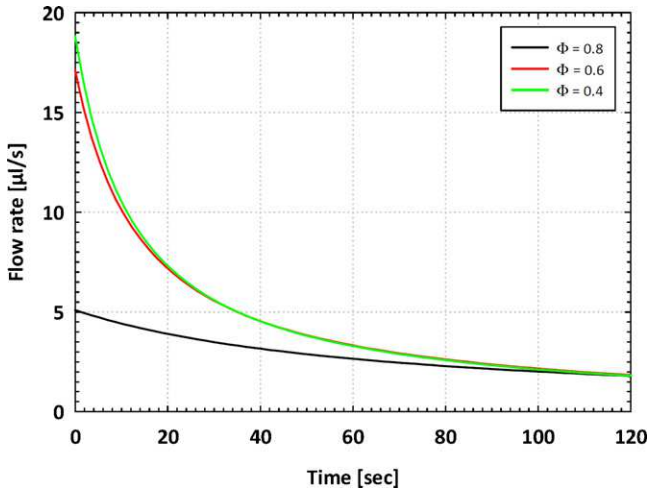

Fig. 7. Evolution of filtration flow rate with time for IO.

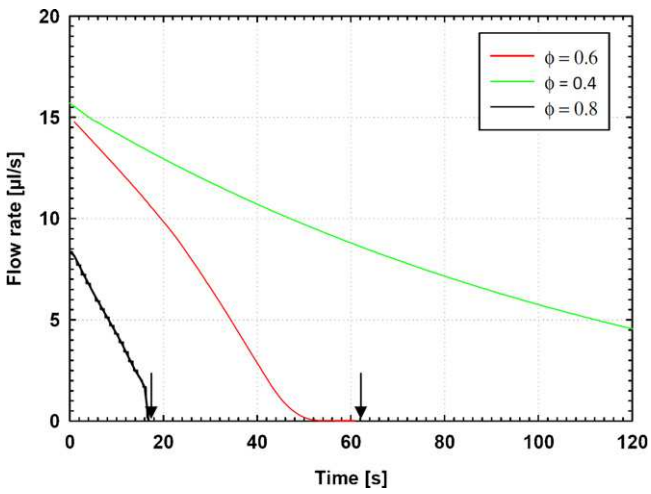

Fig. 8. Evolution of filtration flow rate with time for OI.

was far less than the membrane resistance in the range of time used in this membrane bioreactor [33]. Thus, we can use these simulated profiles and associate them to optimize the operating conditions of a whole cycle of filtration including a one step filtration followed by a backwash step. In this case, the deposit would be formed according to the constraints of the filtration module geometry. The confrontation of the I/O and O/I profiles allow some conclusions to be made and advice to be given. For the inside/out filtration mode and a low packing density ($\Phi = 0.4$) the backwash filtration flow velocity will be higher at the top of the fiber leading to better removal of the cake deposit in this area. For higher fiber packing densities ($\Phi = 0.8$), the backwash flow velocity will be higher at the bottom of the fiber leading to better removal of the deposit in this area. The same conclusions are reached for the outside/in filtration mode.

In this study, simplified model conditions have been selected and particles have been considered inert and monodispersed. Obviously, in the objective of an application to filtration of real microorganisms, other phenomena should be taken into consideration depending on the particle characteristics (size, shape, chemical interactions with the membrane,. . .) and will be the aim of further work.

5. Conclusion

The effect packing density has on spatial cake growth along the fiber was studied using a general handling two dimensional axisymmetric model which considers a coupled physical problem of fluid flow in a channel and through a porous media with an original method to account for cake growth. For simplicity, cake properties like compressibility, specifics of the feed and non-convective transport phenomena were not included. A non-uniform filtration velocity along the fiber is ubiquitous in hollow fiber filtration and leads to uneven particle deposition and cake growth. The model shows an inversed particle deposition pattern at the highest packing density considered, compared with the lowest packing density, in which the fibers can be considered individually. This leads to higher particle deposition at the bottom of the fiber for both the outside/in and inside/out filtration modes. Finally, the results show that a moderate packing density leads to a higher filtration flux and a more homogeneous axial flux profile along the fiber.

This approach highlights the interest of models describing flows and cake growth in hollow fiber filtration modules as a powerful tool for analyzing the effect of the filtration device geometry on the filtration performance. This approach is therefore useful in the design of these filtration devices.

Nomenclature

C_p	particle concentration (kg/m^3)
D	thickness of the fluid envelope (m)
d_p	particle diameter (m)
e_C	thickness of the cake layer (m)
e_m	thickness of the membrane (m)
e_t	total thickness of the porous domain (m)
IO	inside/out filtration mode
K_m	permeability of the membrane (m^2)
K_t	total permeability of the porous domain (m^2)
k	Boltzman constant (J/K)
L	length of the fiber (m)
M	membrane or porous sub domain
m_p	mass of particle deposited per unit area (kg/m^2)
OI	outside/in filtration mode
P	pressure (bar)
P_e	Peclet number
$P_L - P_0$	net pressure drop in the module (bar)
r_i	inner fiber radius (m)
r_e	outer fiber radius (m)
R_c	cake resistance (m^{-1})
R_m	membrane resistance (m^{-1})
R_t	total resistance (m^{-1})
S_t	Stokes number
T	temperature (K)
u	velocity (m/s)

Superscripts

i	inner fluid region
p	porous fluid region
o	outer fluid region

Greek symbols

ΔP_l	local transmembrane pressure (bar)
ε_c	porosity of the cake layer
ε	porosity
μ	dynamic viscosity (Pa s)
μ_{eff}	effective dynamic fluid viscosity (Pa s)
Φ	packing density
ρ_p	particle density (kg/m^3)

References

[1] J. Günther, P. Schmitz, C. Albasi, C. Lafforgue, A numerical approach to study the impact of packing density on fluid flow distribution in hollow fiber module, J. Membr. Sci. 348 (1–2) (2010) 277.
[2] J. Busch, A. Cruse, W. Marquardt, Modeling submerged hollow-fiber membrane filtration for wastewater treatment, J. Membr. Sci. 288 (1–2) (2007) 94.
[3] A.P.S. Yeo, A.W.K. Law, A.G. Fane, Factors affecting the performance of a submerged hollow fiber bundle, J. Membr. Sci. 280 (1–2) (2006) 969.
[4] B. Girard, L.R. Fukumoto, Membrane processing of fruit juices and beverages: a review, Crit. Rev. Food Sci. Nutr. 40 (2000) 91.
[5] E. Salgado Manjarrez, C. Albasi, J.P. Riba, A two-reservoir, hollow-fiber bioreactor for the study of mixed-population dynamics: Design aspects and validation of the approach, Biotechnol. Bioeng. 69 (4) (2000) 401–408.
[6] S. Chang, A.G. Fane, The effect of fibre diameter on filtration and flux distribution – relevance to submerged hollow fibre modules, J. Membr. Sci. 184 (2) (2001) 221.
[7] J. Wu, V. Chen, Shell-side mass transfer performance of randomly packed hollow fiber modules, J. Membr. Sci. 172 (1–2) (2000) 59.
[8] S.-H. Yoon, H.-S. Kim, I.-T. Yeom, Optimization model of submerged hollow fiber membrane modules, J. Membr. Sci. 234 (1–2) (2004) 147.
[9] J.-M. Zheng, Z.-K. Xu, J.-M. Li, S.-Y. Wang, Y.-Y. Xu, Influence of random arrangement of hollow fiber membranes on shell side mass transfer performance: a novel model prediction, J. Membr. Sci. 236 (1–2) (2004) 145.
[10] P.M. Salmon, S.B. Libicki, C.R. Robertson, A theoretical investigation of convective transport in the hollow-fiber reactor, Chem. Eng. Commun. 66 (1988) 221.
[11] L.J. Kelsey, M.R. Pillarella, A. Zydney, Theoretical analysis of convective flow profiles in a hollow-fiber membrane bioreactor, Chem. Eng. Sci. 45 (1990) 3211.
[12] J.D. Rogers, R.L. Long Jr., Modeling hollow fiber membrane contactors using film theory, voronoi tessellations, and facilitation factors for systems with interface reactions, J. Membr. Sci. 134 (1997) 1.
[13] L. Bao, G.G. Lipscomb, Mass transfer in axial flows through randomly packed fiber bundles with constant wall concentration, J. Membr. Sci. 204 (2002) 207.
[14] S. Mahesh Kumar, S. Roy, Filtration characteristics in dead-end microfiltration of living *Saccharomyces cerevisiae* cells by alumina membranes, Desalination 229 (1–3) (2008) 348.
[15] R.M. McDonogh, C.J.D. Fell, A.G. Fane, Surface charge and permeability in the ultrafiltration of non-flocculating colloids, J. Membr. Sci. 21 (3) (1984) 285.
[16] K. Damak, A. Ayadi, B. Zeghmati, P. Schmitz, A new Navier–Stokes and Darcy's law combined model for fluid flow in crossflow filtration tubular membranes, Desalination 161 (1) (2004) 67.
[17] W.N. Gill, D.E. Wiley, C.J.D. Fell, A.G. Fane, Effect of viscosity on concentration polarization in ultrafiltration, AIChE 34 (9) (1988) 1563–1567.

[18] S.K. Karode, Laminar flow in channels with porous walls, revisited, J. Membr. Sci. 191 (1–2) (2001) 237.
[19] V. Nassehi, Modelling of combined Navier–Stokes and Darcy flows in crossflow membrane filtration, Chem. Eng. Sci. 53 (6) (1998) 1253.
[20] S.-H. Yoon, S. Lee, I.-T. Yeom, Experimental verification of pressure drop models in hollow fiber membrane, J. Membr. Sci. 310 (1–2) (2008) 7.
[21] V.N. Kabadi, M.R. Doshi, W.N. Gill, Radial flow hollow fiber reverse osmosis: experiments and theory, Chem. Eng. Commun. 3 (4) (1979) 339–365.
[22] L. Brinkert, P. Paris, M. Renner, J.M. Espenan, P. Aptel, Pressure drops in radial flow membrane modules for ultrafiltration hollow fibers, J. Membr. Sci. 92 (2) (1994) 131.
[23] J. Günther, C. Albasi, C. Lafforgue, Filtration characteristics of hollow fiber microfiltration membranes used in a specific double membrane bioreactor, Chem. Eng. Process. Proc. Int. 48 (7) (2009) 1255.
[24] J. Happel, Viscous flow relative to arrays of cylinders, AIChE J. 5 (2) (1959) 174–177.
[25] P. Schmitz, M. Prat, 3-D laminar stationary flow over a porous surface with suction: description at pore level, AIChE J. 41 (10) (1995) 2212–2226.
[26] J. Dufrèche, M. Prat, P. Schmitz, Effective hydraulic resistance of the first cake layers at the membrane surface in microfiltration, Desalination 145 (1–3) (2002) 129.
[27] D. Gassara, P. Schmitz, A. Ayadi, M. Prat, Modelling the effect of particle size in microfiltration, Sep. Sci. Technol. 43 (7) (2008) 1754–1770.
[28] F.A.L. Dullien, Porous media: fluid transport and pore structure, Academic Press, New York, 1979, p. 396.
[29] M. Elimelech, Particle deposition and aggregation: measurement, modelling and stimulation, Colloids Surf. Eng. Ser. (1995).
[30] J. Mendret, Mise au point de méthodes de caractérisation du colmatage de membranes: application à la caractérisation in situ d'un dépôt particulaire en ultrafiltration frontale en lien avec les performances du procédé, Thesis, INSA, Université de Toulouse, 2007.
[31] T. Carroll, The effect of cake and fibre properties on flux declines in hollow-fibre microfiltration membranes, J. Membr. Sci. 189 (2) (2001) 167.
[32] J. Kincl, P. Dolecek, J. Cakl, Filtration model for hollow fiber membranes with compressible cake formation, Desalination 240 (1–3) (2009) 99.
[33] J. Günther, Caractérisation et optimisation des phénomènes de transfert dans un double bioréacteur à membranes, Thesis, ENSIACET, Université de Toulouse, 2009.
[34] H. Lange, P. Taillandier, J.P. Riba, Effect of high shear stress on microbial viability, J. Chem. Tech. Biotech. 76 (2001) 501–505.